



Pressure level of maximum radiative heating enhancement in response to increasing CO₂ over the global monsoon area

CO₂浓度增加背景下季风区大气辐射加热响应的差异

Xia Qu^{a,b,*}, Gang Huang^{b,c,d}, Xiaocong Wang^b

^a Center for Monsoon System Research, Institute of Atmospheric Physics, Chinese Academy of Sciences, Beijing, China

^b State Key Laboratory of Numerical Modeling for Atmospheric Sciences and Geophysical Fluid Dynamics, Institute of Atmospheric Physics, Chinese Academy of Sciences, Beijing, China

^c Laboratory for Regional Oceanography and Numerical Modeling, Qingdao National Laboratory for Marine Science and Technology, Qingdao, China

^d University of Chinese Academy of Sciences, Beijing, China

ARTICLE INFO

Keywords:

Radiative heating
Increasing CO₂
Global monsoon area
Cloud
关键词:
大气辐射加热
季风区
CO₂
云

ABSTRACT

Based on the 1%CO₂ experiment of CMIP6, in response to increasing CO₂, the summer-mean radiative heating (RH) over the global monsoon area (MA) generally features an increasing response in the mid-troposphere and a decreasing response in the lower and upper troposphere. The pressure level of the maximum RH increase over the Asian MA is the highest and largest in range (500–775 hPa); the maximum increases over the North African, South American, and Australian MA are at 550–600 hPa; throughout the North American MA, the maximum heating increase is at 600 hPa; and the levels of the maximum over South Africa are 600 and 775 hPa. For most of the global MA, the maximum enhancement of RH is at 500, 550, and 600 hPa. It is mainly led by the increase in cloud water at and above the maximum level and the decrease in cloud water below, which leads to similar changes in total cloud mass. Because of the longwave heating (cooling) effect at the cloud base (top), the RH enhancements peak at those levels. For the northeast part of the Asian MA and southeast part of the South African MA, RH enhancement peaks at 700 and 775 hPa, mainly attributable to the cloud water reduction below. The reduction leads to similar changes in total cloud. Due to the longwave cooling effect at the cloud top, the reduction contributes to the RH enhancement at the corresponding maximum levels.

摘要

大气CO₂浓度增加, 大气辐射平衡调整, 将影响到大气的辐射加热, 对季风环流的产生影响。CMIP6结果显示, 大气CO₂浓度增加, 可减弱季风区主雨季对流层高, 低层的辐射加热, 加强对流层中层的辐射加热。各季风区加热响应的峰值层次不同: 亚洲季风区平均层次最高 (500-775 hPa), 北非, 南美, 澳洲季风区次之 (550-600 hPa), 北美 (600 hPa) 和南非季风区 (600-775 hPa) 较低。各季风区水云的垂直分布及其长波辐射效应的变化是形成峰值层次差异的主因。

1. Introduction

Heating is an important factor driving the atmospheric circulation (Gill, 1980; Matsuno, 1966). It is composed of latent heating and radiative heating (RH) (Luo and Yanai, 1984; Nitta, 1972; Yanai et al., 1973). The former is associated with water condensation and has been relatively well studied; whereas, the latter, which is related to the shortwave and longwave radiation received and emitted by the atmosphere, has been somewhat overlooked.

Since the Industrial Revolution, the CO₂ concentration in the atmosphere has been increasing. This increase redistributes the energy over

the globe and has a profound influence on climate (Stocker et al., 2013). When CO₂ radiative forcing enhances, the increased rate of global precipitation cannot keep pace with that of moisture, resulting in a slowdown of the atmospheric circulation (Held and Soden, 2006; Vecchi and Soden, 2007). This slowdown occurs over most of the global monsoon area (MA), where climatological ascendance prevails (Endo et al., 2018). One exception is the South Asian MA, where the slowdown is inapparent. Endo and Kitoh (2014) proposed that this inapparent is linked to the relatively larger quantities of precipitation there. Meanwhile, relative to the other MAs, over the Asian MA, the stronger latent heating associated with the precipitation and the weaker slowdown are coupled, making it hard to explore the causes of the unique slowdown response.

* Corresponding author.

E-mail address: quxia@mail.iap.ac.cn (X. Qu).

<https://doi.org/10.1016/j.aosl.2021.100037>

Received 9 August 2020; Revised 11 September 2020; Accepted 12 October 2020

Available online 4 February 2021

1674-2834/© 2021 The Authors. Published by Elsevier B.V. on behalf of Institute of Atmospheric Physics, Chinese Academy of Sciences. This is an open access article under the CC BY-NC-ND license (<http://creativecommons.org/licenses/by-nc-nd/4.0/>)

Table 1 Information on the climate models used in this study.

No.	Model ID	Modeling center (or group)	Run
1	CESM2	National Center for Atmospheric Research, USA	r1i1p1f1
2	CESM2-FV2		r1i1p1f1
3	CESM2-WACCM		r1i1p1f1
4	CESM2-WACCM-FV2		r1i1p1f1
5	CNRM-CM6-1	Centre National de Recherches Météorologiques, Centre Européen de Recherche et de Formation Avancée en Calcul Scientifique, France	r1i1p1f2
6	CNRM-ESM2-1	Atmosphere and Ocean Research Institute (The University of Tokyo), National Institute for Environmental Studies, and Japan Agency for MRO5 Marine-Earth Science and Technology, Japan	r1i1p1f2
7	MIROC-ES2L		r1i1p1f1
8	MIROC6		r1i1p1f1
9	MPI-ESM-1-2-HAM	Max Planck Institute for Meteorology	r1i1p1f1
10	MPI-ESM1-2-LR		r1i1p1f1

Therefore, studying the changes in another form of heating (namely, RH) might be beneficial to our understanding of climate change over the South Asian MA, as well as the global MA.

As the global temperature or CO₂ radiation increases, there is evidence to suggest that the atmospheric RH may change. First, global warming may lead to increased high-level cloud and reduced mid- and low-level cloud (Boucher et al., 2013; Hartmann and Larson, 2002). This may alter the vertical profile of RH (Dolinar et al., 2019; Li et al., 2013). Second, the atmospheric warming, a result of increasing CO₂, may lead to moistening of the atmosphere and thus induce stronger absorption of longwave and shortwave radiation (Wild et al., 2013). Third, according to Stefan–Boltzmann’s law, warming in the atmosphere slightly enhances its radiative cooling effect. Nevertheless, how the RH behaves over the global MA is not clear—a gap in knowledge that the present paper seeks to address.

Following this introduction, section 2 introduces the data and methods. Section 3 presents the results on the pressure levels of maximum RH increase during local summer over the global MA. Section 4 provides a summary and discussion.

2. Data and methods

2.1. Data

The present study is based on monthly outputs of CMIP6 models (Eyring et al., 2016). Information on the models is provided in Table 1. The experiment used is the 1%CO₂ experiment, in which the coupled general circulation models are forced by CO₂ increases of 1% per year until the CO₂ concentration is quadrupled. Only the first run (the name of the run is also listed in Table 1) is analyzed.

The climate change over the global MA in our real climate, rather than in the simulation, is of significance and is our focus. To obtain the global MA, the following observational data are used: (1) Global Precipitation Climatology Project, version 2.3 (Adler et al., 2003); and (2) Center for Climate Prediction Merged Analysis of Precipitation (Xie and Arkin, 1997). Both sets of precipitation data have a 2.5° horizontal resolution. The focus is on the period 1980–2005.

2.2. Methods

The response to increasing CO₂ is defined as the difference between the climatology during the 121st–140th year and that during the 1st–20th year in the 1%CO₂ experiment. To study the responses of the CMIP6 models, this study uses the multi-model ensemble (MME) method. The 95% confidence intervals among the models are used to identify the significance of the signal. To facilitate the analysis of the MME and the confidence intervals, we use a bilinear interpolation technique to interpolate the data onto a 1.0° × 1.0° grid. Note that the interpolation is not performed when we compute the area average. Most

of the RH results are in hybrid sigma-pressure coordinates, which has a more sophisticated vertical level than the conventional pressure coordinate. To obtain detailed information, we interpolate the results into a pressure coordinate whose levels are 1000, 925, 850, 775, 700, 650, 600, 550, 500, 450, 400, 350, 300, 250, 200, 150, 100, 70, 50, 30, 20, and 10 hPa.

The definition of the global MA follows that of Wang and Ding (2008) and Hsu et al. (2013). It is defined as the domains where the difference between local summer and local winter mean precipitation exceeds 2 mm d⁻¹, and the total precipitation in local summer accounts for no less than 55% of annual rainfall. In the Northern Hemisphere, the definition of local summer is May to September, and the local winter is November to March; in the Southern Hemisphere, the definition is the reverse. At the equator the result is set to null. The boundaries of the global MA are displayed in Fig. 1 as thick black lines. In this study, the local summer results are our focus.

3. Results

3.1. Overall features

In response to increasing CO₂, summer-mean RH generally features an increasing response in the mid-troposphere and a decreasing response in the lower and upper troposphere. Fig. 1 displays the responses of RH from 400 to 850 hPa. At 400 and 850 hPa, over the majority of the global MA, the RH undergoes a decline (Fig. 1(a, h)). At 500 hPa, increases in RH are found over the Asian, North African, South American and eastern part of the Australian MA, with maximum heating enhancement over the Tibetan Plateau (~0.5 K d⁻¹); decreases are found over the South African and northeastern part of the Asian MA (Fig. 1(b)). At 550 hPa, significant enhancement of RH occurs over all the MAs except the northeastern part of the Asian MA (Fig. 1(c)). Larger enhancements reside over Indochina and the equatorial sides of the North African, South African, North American and South American MA. At 600 hPa, the majority of the global MA features a rise in RH. The magnitudes are relatively large over the inland African and South American MA (Fig. 1(d)). At 650 hPa, the magnitudes of the RH change over the global MA are slightly weaker (Fig. 1(e)). At 700 hPa, the equatorial sides of the global MA undergo a decline in RH; the RH increases exist over the polar sides of the global MA, except the North African MA (Fig. 1(f)). The behavior of the RH at 775 hPa is similar, but the increase disappears over the northern edge of the Australian MA (Fig. 1(g)).

The level of maximum RH enhancement varies across the global MA. Fig. 2 displays the level of maximum increase in RH over the global MA. In response to increasing CO₂, the level of the maximum increase over the Tibetan Plateau is generally the highest among the MAs, with the level at 500 hPa (Fig. 2). It is probably affected by the local topography. For the maximum heating response residing at 550 hPa, the areas locate over the majority of the Asian MA south of 30°N, in the south

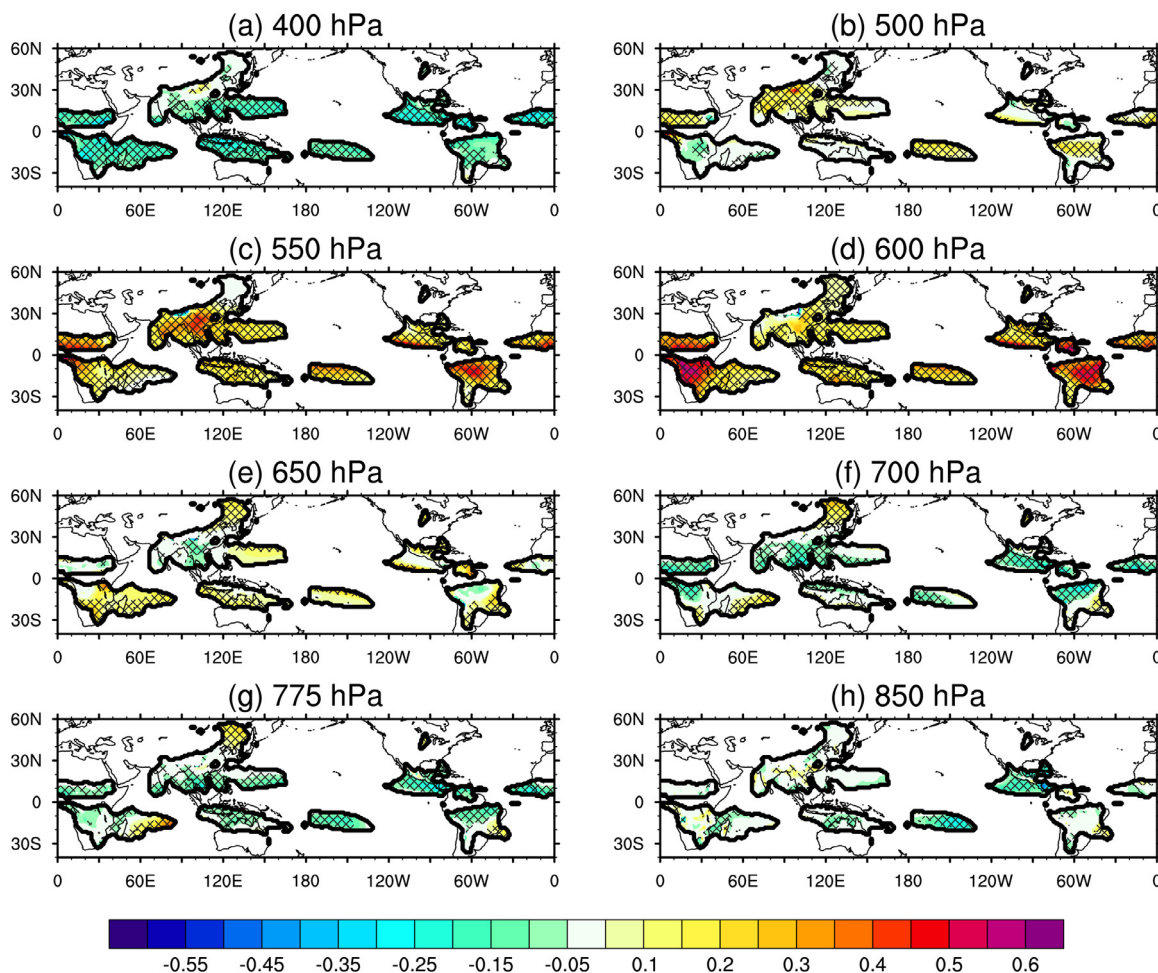


Fig. 1. The MME responses of RH at (a) 400, (b) 500, (c) 550, (d) 600, (e) 650, (f) 700, (g) 775, and (h) 850 hPa, over the global MA (boundaries indicated by thick lines). Units: $K d^{-1}$. The lattice patterns indicate areas where the response reaches the 95% confidence level.

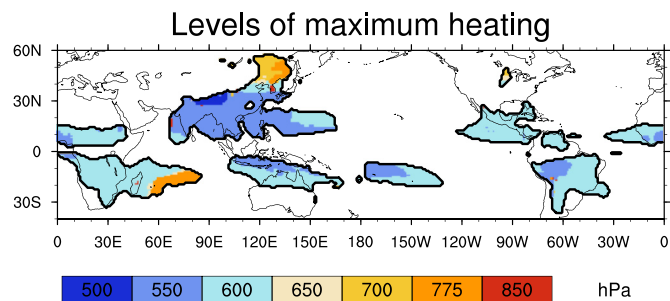


Fig. 2. Map of the levels of maximum increase in RH based on the MME result.

or southwest part of the Australian MA, and the equatorial sides of the African MA and South American MA. For most of the global MA, except the Asian MA, the enhancement of RH peaks at 600 hPa; and this kind of RH also occurs near 40°N of and over the east of the Asian MA. Over the northeast part of the Asian MA, a maximum increase at 700 hPa is found. Over the eastern edge of both the South African MA and northeast Asian coast, the RH increase peaks at 775 hPa. In general, the level of maximum RH increase over the Asian MA is the highest, and has the largest pressure-level range among the global MAs; the North African, South American and Australian MAs feature maximum RH increases at 550–600 hPa; throughout the North America MA, the maximum heating

enhancement exists at 600 hPa; and the pressure level of the maximum heating increase over South Africa is mainly at 600 and 775 hPa.

To further investigate the vertical structure and possible cause, based on the levels of maximum RH enhancement, the global MA is sorted into the following categories: maximum enhancement at 500, 550, 600, 700, or 775 hPa. Based on these categories, the averaged vertical profiles of the RH response are displayed in Fig. 3. As the maximum enhancement of RH at 500, 550, or 600 hPa occurs over the majority of the global MA and share similar features, the RH response and possible causes are discussed together. Likewise, the behaviors of the RH and associated variables over the areas of maximum enhancement of RH at 700 and 775 hPa bear resemblance, and thus these two are also discussed together. This kind of RH response mainly exists over the northeast part of the Asian MA and southeast part of the South African MA.

3.2. Maximum enhancement of RH at 500, 550, and 600 hPa

For the RH enhancement peaks at 500 hPa, slight intensification of RH also occurs at approximately 50 hPa; strong cooling responses are found at 650 and 150 hPa (Fig. 3(a)). The occurrence of results below 800 hPa is due to the fact that the maximum surface pressures over some grid points are greater than 800 hPa in some models. The vertical profile of the responses of longwave RH and shortwave RH (denoted as thin solid and dashed lines in Fig. 3(a)) reveals that longwave RH mainly accounts for the total RH response; the shortwave response partly cancels out the RH response.

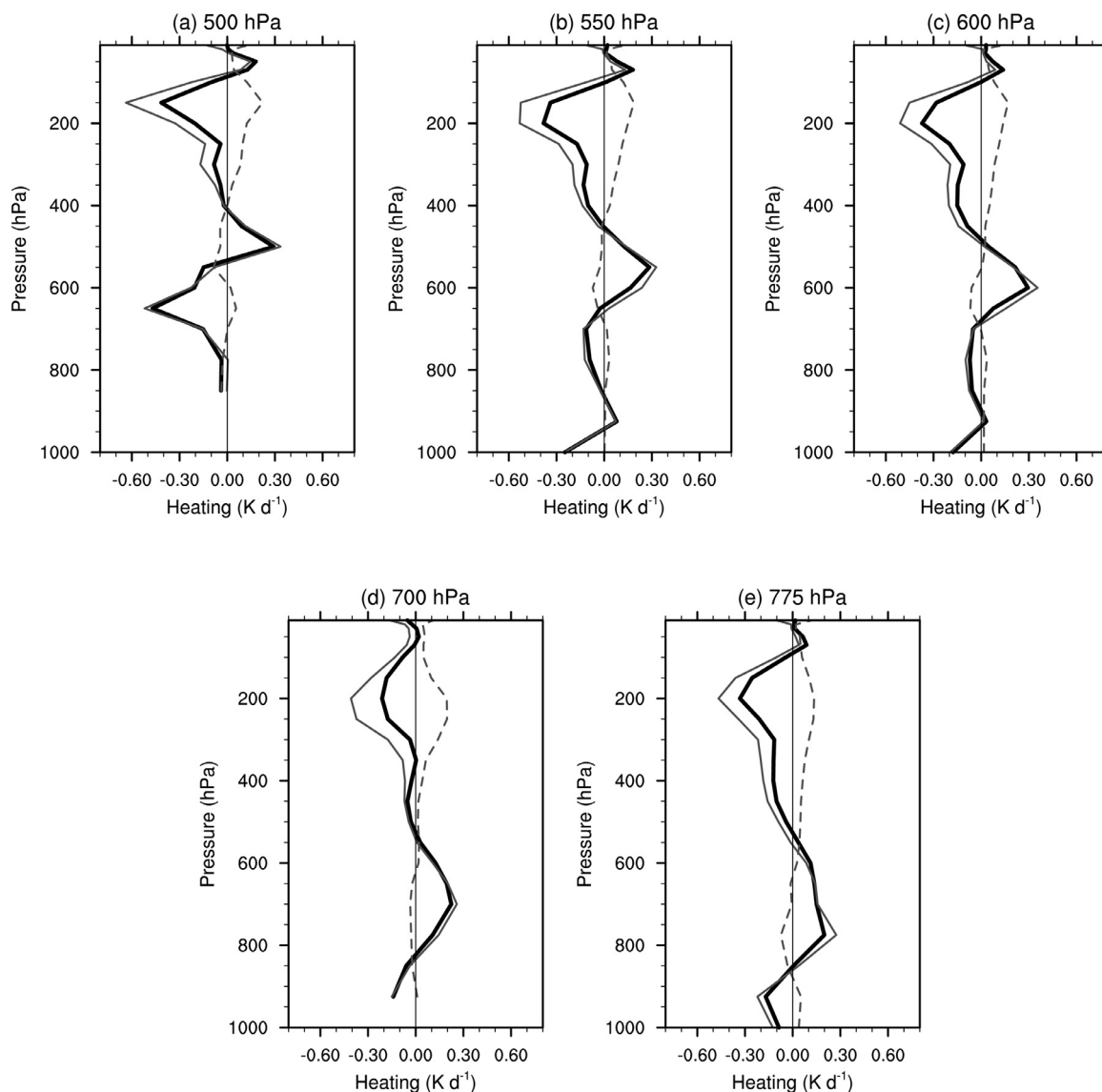


Fig. 3. Vertical profiles of the responses of the total RH (thick solid lines), longwave RH (thin solid lines), and shortwave RH (thin dashed lines) at (a) 500, (b) 550, (c) 600, (d) 700, and (e) 775 hPa, in the MME result. Units: K d^{-1} .

For the longwave RH response in the mid-troposphere, cloud change is mainly responsible. Fig. 4(a) displays the response of total cloud mass fraction. For the RH enhancement peaks at 500 hPa, an increase in total cloud mass is found at and above 500 hPa. Because of the longwave heating and cooling effect at the cloud base and top (Chen and Cotton, 1987), the increase in cloud at and above 500 hPa contributes to an increase in longwave heating at or slightly below 500 hPa. Besides, a decrease in total cloud mass occurs at 550 hPa, and this also contributes to the longwave heating slightly above it. Thus, the longwave heating, as well as the total RH, intensifies at 500 hPa.

Cloud water is mainly accountable for the vertical profile of the change in cloud. The total cloud mass is composed of the mass of cloud water and ice. The vertical profile of the cloud water response is similar to that of the total cloud mass response, but the increase in cloud water is greater (Fig. 4(a)). The cloud ice displays a reduction below 150 hPa and intensification above 150 hPa.

Regarding the cloud water and ice response to increasing CO_2 , the former is explainable. Cloud ice usually forms at a relatively fixed temperature (Hartmann and Larson, 2002). In response to increasing CO_2 , the troposphere warms and the height of the “fixed temperature” ele-

vates. Consequently, the height of cloud ice rises, corresponding to the reduction of cloud ice in the mid to lower troposphere and the increase in the upper troposphere. Meanwhile, because of the lack of model outputs associated with cloud water generation, it is difficult to diagnose the change in cloud water.

With respect to the maximum increase of RH at 550 and 600 hPa, the responses of the cloud and RH are similar, except that the level of the vertical structure differs slightly (Figs. 3(b, c) and 4(b, c)).

3.3. Maximum enhancement of RH at 700 and 775 hPa

Like the results at 500 to 600 hPa, this kind of RH enhancement features an increase in RH near the top of the troposphere and a reduction in the upper and lower troposphere (Fig. 3(d)). The increase in RH is mainly led by changes in longwave RH. Furthermore, the reduced cloud water at 775 hPa is mainly responsible for it (Fig. 4(d)). It decreases the total cloud mass and weakens the longwave cooling effect at the cloud top. Thus, the maximum RH enhancement occurs at 700 hPa.

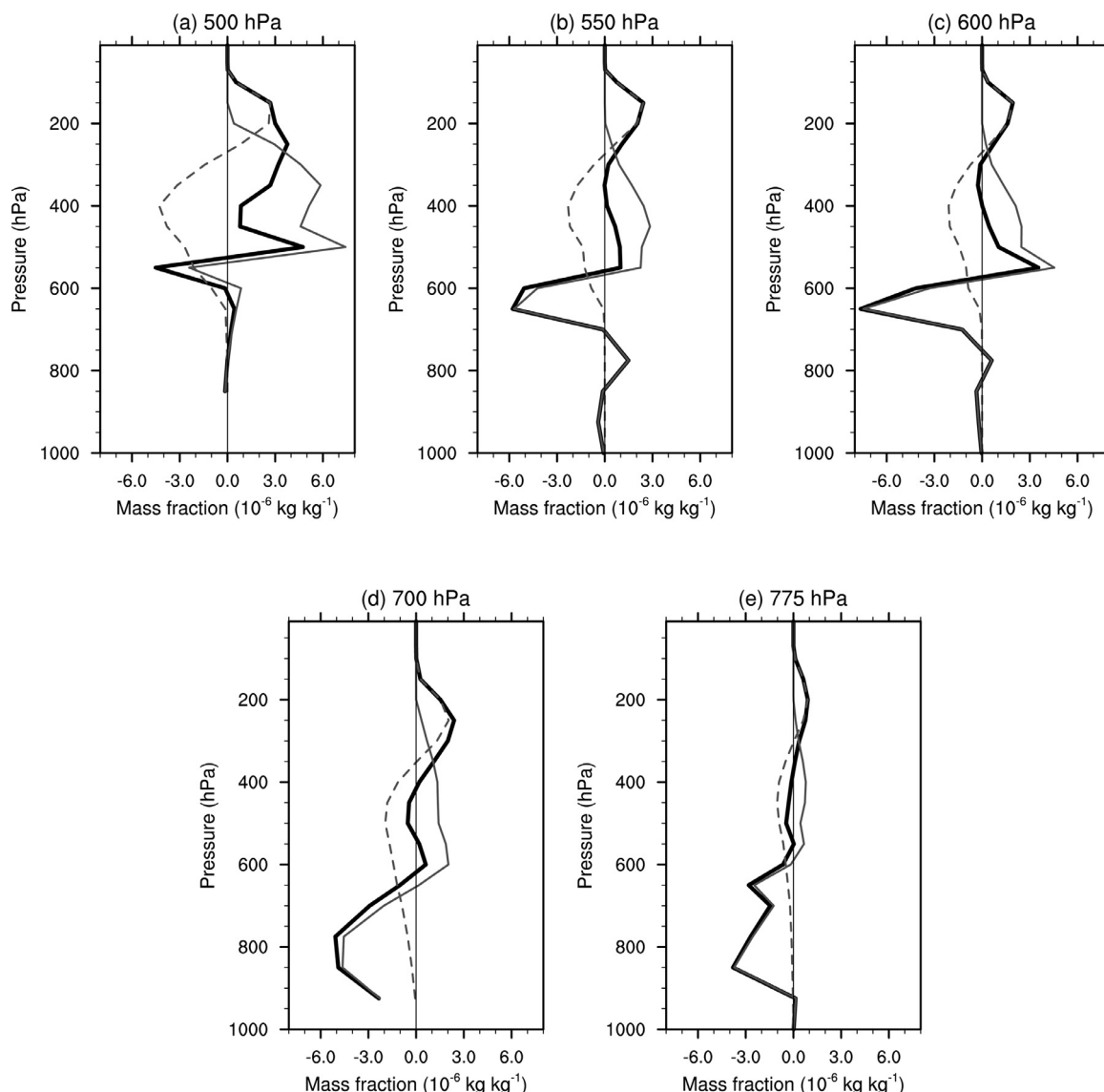


Fig. 4. Vertical profiles of the mass fraction responses of the cloud water (thin solid lines) and cloud ice (thin dashed lines) at (a) 500, (b) 550, (c) 600, (d) 700, and (e) 775 hPa, in the MME result. The thick black lines are the sum of cloud water and cloud ice. Units: kg kg^{-1} .

Regarding the maximum enhancement of RH at 775 hPa, the vertical structure is similar. Likewise, the enhancement can be explained by the reduction of underlying cloud water (Figs. 3(e) and 4(e)).

4. Summary

The output of the 1%CO₂ experiment suggests that, in response to increasing CO₂, over the global MA, the summer-mean RH generally features an increased maximum in the mid-troposphere and a decrease in the lower and upper troposphere. The pressure level of the maximum RH increase over the Asia MA is the highest, and has the widest range among the global MAs (500–775 hPa); over the North African, South American, and Australian MAs, the maximum RH enhancement is at 550–600 hPa; throughout the North American MA, the maximum enhancement is at 600 hPa; and the maximum enhancement over South Africa exists at 600 and 775 hPa.

Based on the levels of maximum RH increase, the global MA is sorted into the following categories: maximum RH increases at 500, 550, 600, 700, or 775 hPa. Over the majority of the global MA, the RH enhancement peaks at 500, 550, and 600 hPa. It is mainly led by an increase in cloud water at and above that level and a decrease at the level below.

Consequently, the total cloud mass displays a similar response. Due to the longwave radiative heating (cooling) effect at the cloud base (top), the RH enhancements peak at the “peak” levels. Over the northeast part of the Asian MA and southeast part of the South African MA, the RH enhancement peaks at 700 and 775 hPa, and this is mainly induced by the decrease in cloud water below. The decrease leads to the similar response of the total cloud. Due to the longwave cooling effect at the cloud top, the decrease in cloud contributes to the RH enhancement at the “peak” levels.

Funding

The study was supported by the National Natural Science Foundation of China [grant numbers 41831175 and 41530425], the Strategic Priority Research Program of the Chinese Academy of Sciences [grant number XDA20060501], the Key Deployment Project of the Centre for Ocean Mega-Research of Science, Chinese Academy of Sciences [grant number COMS2019Q03], and the Second Tibetan Plateau Scientific Expedition and Research (STEP) program [grant number 2019QZKK0102].

Acknowledgments

We acknowledge the World Climate Research Programme, which, through its Working Group on Coupled Modelling, coordinated and promoted CMIP6. We thank the climate modeling groups for producing and making available their model output, the Earth System Grid Federation (ESGF) for archiving the data and providing access, and the multiple funding agencies who support CMIP6 and ESGF.

References

- Adler, R.F., Huffman, G.J., Chang, A., Ferraro, R., Xie, P.P., Janowiak, J., Rudolf, B., et al., 2003. The version-2 global precipitation climatology project (GPCP) monthly precipitation analysis (1979-present). *J. Hydrometeorol.* 4, 1147–1167.
- Boucher, O., Randall, D., Artaxo, P., Bretherton, C., Feingold, G., Forster, P.M., Kerminen, V.-M., et al., 2013. Clouds and aerosols. In: Stocker, T.F., et al. (Eds.), *Climate Change 2013: The Physical Science Basis. Contribution of Working Group I to the Fifth Assessment Report of the Intergovernmental Panel on Climate Change*. Cambridge University Press, 593. Cambridge, United Kingdom and New York, NY, USA.
- Chen, C., Cotton, W.R., 1987. The physics of the marine stratocumulus-capped mixed layer. *J. Atmos. Sci.* 44, 2951–2977.
- Dolinar, E.K., Dong, X.Q., Xi, B.K., Jiang, J.H., Loeb, N.G., Campbell, J.R., Su, H., 2019. A global record of single-layered ice cloud properties and associated radiative heating rate profiles from an A-Train perspective. *Clim. Dyn.* 53, 3069–3088.
- Endo, H., Kitoh, A., 2014. Thermodynamic and dynamic effects on regional monsoon rainfall changes in a warmer climate. *Geophys. Res. Lett.* 41, 1704–1710.
- Endo, H., Kitoh, A., Ueda, H., 2018. A unique feature of the Asian summer monsoon response to global warming: the role of different land-sea thermal contrast change between the lower and upper troposphere. *SOLA* 14, 57–63.
- Eyring, V., Bony, S., Meehl, G.A., Senior, C.A., Stevens, B., Stouffer, R.J., Taylor, K.E., 2016. Overview of the coupled model intercomparison project phase 6 (CMIP6) experimental design and organization. *Geosci. Model Devel.* 9, 1937–1958.
- Gill, A.E., 1980. Some simple solutions for heat-induced tropical circulation. *Q. J. R. Meteorolog. Soc.* 106, 447–462.
- Hartmann, D.L., Larson, K., 2002. An important constraint on tropical cloud—climate feedback. *Geophys. Res. Lett.* 29 (20), 1951. doi:10.1029/2002GL015835.
- Held, I.M., Soden, B.J., 2006. Robust responses of the hydrological cycle to global warming. *J. Clim.* 19, 5686–5699.
- Hsu, P.C., Li, T., Murakami, H., Kitoh, A., 2013. Future change of the global monsoon revealed from 19 CMIP5 models. *J. Geophys. Res.-Atmosph.* 118, 1247–1260.
- Li, W., Schumacher, C., McFarlane, S.A., 2013. Radiative heating of the ISCCP upper level cloud regimes and its impact on the large-scale tropical circulation. *J. Geophys. Res.-Atmosph.* 118, 592–604.
- Luo, H., Yanai, M., 1984. The large-scale circulation and heat sources over the Tibetan plateau and surrounding areas during the early summer of 1979. Part II: heat and moisture budgets. *Mon. Wea. Rev.* 112, 966–989.
- Matsuno, T., 1966. Quasi-geostrophic motions in the equatorial area. *J. Meteorol. Soc. Japan* 44, 25–43.
- Nitta, T., 1972. Energy budget of wave disturbances over the Marshall Islands during the years of 1956 and 1958. *J. Meteorol. Soc. Japan* 50, 71–84.
- Stocker, T.F., Qin, D., Plattner, G.K., Alexander, L.V., Allen, S.K., Bindoff, N.L., Bréon, F.M., et al., 2013. Technical summary. In: Stocker, T.F., et al. (Eds.), *Climate Change 2013: The Physical Science Basis. Contribution of Working Group I to the Fifth Assessment Report of the Intergovernmental Panel on Climate Change*. Cambridge University Press, 79. Cambridge, United Kingdom and New York, NY, USA.
- Vecchi, G.A., Soden, B.J., 2007. Global warming and the weakening of the tropical circulation. *J. Clim.* 20, 4316–4340.
- Wang, B., Ding, Q.H., 2008. Global monsoon: dominant mode of annual variation in the tropics. *Dyn. Atmos. Oceans* 44, 165–183.
- Wild, M., Folini, D., Schar, C., Loeb, N., Dutton, E.G., König-Langlo, G., 2013. The global energy balance from a surface perspective. *Clim. Dyn.* 40, 3107–3134.
- Xie, P.P., Arkin, P.A., 1997. Global precipitation: a 17-year monthly analysis based on gauge observations, satellite estimates, and numerical model outputs. *Bull. Am. Meteorol. Soc.* 78, 2539–2558.
- Yanai, M., Esbensen, S., Chu, J.H., 1973. Determination of bulk properties of tropical cloud clusters from large-scale heat and moisture budgets. *J. Atmos. Sci.* 30, 611–627.